LAWRENCE
LIVERMORE
NATIONAL
LABORATORY

LLNL-CONF-440992

Exploring Crystal Plasticity Via Far-Field 3DXRD

J. V. Bernier, N. R. Barton, M. C. Brandes, U. Lienert, M. P. Miller, M. J. Mills

July 9, 2010

31st Risø International Symposium on Materials Science: Challenges in materials science and possibilities in 3D and 4D characterization techniques
Roskilde, Denmark
September 6, 2010 through September 10, 2010

Disclaimer

EXPLORING CRYSTAL PLASTICITY VIA FAR-FIELD 3DXRD

J. V. Bernier*, N. R. Barton*, M. C. Brandes†,
U. Lienert‡, M. P. Miller§, and M. J. Mills¶

* Engineering Technologies Division,
Lawrence Livermore National Laboratory, Livermore, CA, USA
† United States Naval Research Laboratory, Washington DC, USA
‡ The Advanced Photon Source,
Argonne National Laboratory, Argonne, IL, USA
§ Sibley School of Mechanical & Aerospace Engineering,
Cornell University, Ithaca, NY, USA
¶ Department of Materials Science & Engineering,
The Ohio State University, Columbus, OH, USA

ABSTRACT

A specimen of Ti-7%Al alloy was subject to tensile deformation *in situ* at APS 1-ID-C. Within it, a neighborhood containing 20 complete grains was indexed in the annealed state and subsequently tracked at several applied stresses during *in situ* loading, both preceding and following the macroscopic yield stress. The stress states of each grain were observed to reorient significantly post yield despite the fact that their average remained close to the applied uniaxial stress. To aid in interpreting the experimental results, a virtual realization of the neighborhood was created using a finite element mesh. Each individual grain was represented by $\sim$ 1000 hexahedral elements. Ensemble averaged resolved shear stresses were calculated over the neighborhood from both the experimental and simulated data. Despite the lack of intra-granular resolution in the experiment – and with the aid of the simulated data – the resolved shear stresses projected on several slip system families are shown to statistically capture the associated critical resolved shear stresses. This important result implies that the far-field 3DXRD method may be applied to the study of specific of slip system activity in embedded neighborhoods of grains subject to thermomechanical processing *in situ*.

1. INTRODUCTION

An empirical understanding of the most important structure/mechanical property relationships exists for many polycrystalline alloys. However, explicit, structure-based prediction of grain scale deformation behavior *within* a polycrystalline aggregate remains a vast research frontier. The relative lack of grain scale experimental data – particularly three-dimensional – has seriously retarded efforts to illuminate and validate micromechanical deformation models. While mechanical tests on large single crystals have provided many critical insights, actual probes of the crystal-scale "stress–strain" response deep within deforming aggregates *in situ* are vitally needed to advance the field. Due to anisotropy in the mechanical properties

of single crystals, as well as inter-granular interactions, significant deformation heterogeneity can exist from one grain to the next in an aggregate even under macroscopically simple loading conditions (*e.g.* uniaxial stress). As evidenced by many recent publications, high energy synchrotron x-ray diffraction experiments employing *in situ* loading hold enormous potential as such grain scale mechanical behavior probes (Margulies, Lorentzen, Poulsen, and Leffers, 2002; Martins, Margulies, Schmidt, Poulsen, and Leffers, 2004; Bernier and Miller, 2006; Bernier, Park, Pilchak, Glavicic, and Miller, 2008; Aydıner, Bernier, Clausen, Lienert, Tomé, and Brown, 2009; Lienert, Brandes, Bernier, Weiss, Shastri, Mills, and Miller, 2009).

The far-field 3DXRD method discussed herein was developed following the work of Poulsen, Nielsen, Lauridsen, Schmidt, Suter, Lienert, Margulies, Lorentzen, and Juul Jensen (2001) and Lauridsen, Schmidt, Suter, and Poulsen (2001). Far-field 3DXRD is a monochromatic, transmitted beam technique that interrogates entire embedded neighborhoods simultaneously. Margulies et al. (2002) and Martins et al. (2004) demonstrated the feasibility of applying the 3DXRD technique for obtaining fully three-dimensional lattice strain tensors for individual grains embedded in polycrystalline speciemens subject to loading *in situ*. It is noted that the technique as presented lacks intra-granular resolution; the orentations and strain tensors obtained are volumetric averages over the individual grains, a condition that puts some restrictions on the gross shape and extent of the measured diffraction spots. In this paper we outline a method for identifying an embedded neighborhood of grains by fitst-pass orientation indexing, determining the center-of-mass coordinates, and finally the refined orientation and mean strain tensor for each grain in the illuminated volume. In particular, the method for calculating a strain measure involves applying finite strain theory in a crystallographically self-consistent manner (*i.e.* under crystal symmetry).

As a demonstration, an example using data from an *in situ* deformation experiment on a specimen of Ti-7%Al alloy (α-Ti, HCP) is provided. These data – and the details of the corresponding experiment – have been previously presented by Lienert et al. (2009). The Ti-7%Al was air-cooled post annealing, which has implications on the relative slip system strengths that will be discussed later. Loading was halted and diffraction data were collected at increasing macroscopic stress values both pre- and post-yield. Titanium is an ideal system for this application due to its large strength to stiffness ratio and low x-ray attenuation. Lattice strains up to nearly 1% are possible with sample sizes over a millimeter (Bernier et al., 2008; Lienert et al., 2009).

This framework is currently being implemented at beamline 1-ID-C at the Advanced Photon Source for determining the centroids, orientations and lattice strain tensors for an aggregate of crystals during thermo-mechanical processing *in situ*. We seek to illustrate the immense potential of combining this experimental capability together with a crystal-based finite element simulation of a virtual realization of the measured aggregate. By integrating these tools it is possible to gleaning far more insight on the deforming aggregate than would be possible through using either technique alone. Similar to the recent work of Winther (2008), it is shown that critical resolved shear stresses – and thus specific slip system activity – may be identified using the far-field 3DXRD technique for specimens deformed *in situ*.

2. FAR-FIELD 3DXRD METHOD

In the far-field geometry, the detector distance is large with respect to the beam dimensions defining diffraction volume. Even with the detector fixed, it has been shown that there is sufficient resolution to determine the centers of mass of equiaxed grains to within 5 μm. The experimental method itself is essentially indistinguishable from the previously presented

3DXRD method, save that the sample-to-detector distance is strictly fixed (Lauridsen et al., 2001; Margulies et al., 2002; Martins et al., 2004). A schematic of the instrument geometry is shown in Fig. 1. Single diffraction images are recorded as the sample is swept through an increment $\Delta\omega$, typical magnitudes of which are $0.1^\circ - 1^\circ$ for an *in situ* experiment. Ideally, $\omega \in [-\pi/2, \pi/2]$, although ancillary equipment such as loadframes or furnaces typically limit the full range to $\leq 120^\circ$.

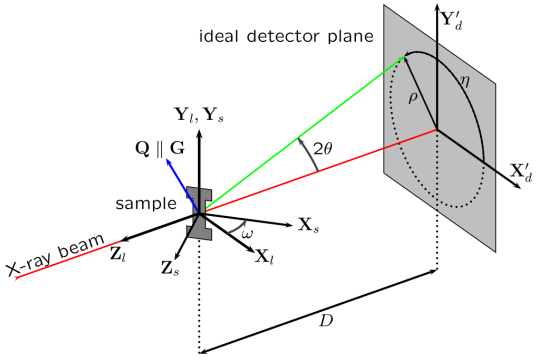

Fig. 1: Schematic of the far-field 3DXRD method.

A thorough exposition of the data analysis method, from image processing to grain indexing and refinement, is outdside the scope of this article and will be provided elsewhere. Some salient points, however, are given below.

- Differential thresholding based on both structure factors (when available) and ω polarization is employed prior to processing the raw images. The expression for the polarization consistent with the geometry of Fig. 1 is $f = \sqrt{\sin\theta^2 + \cos\eta^2 \cos\theta^2}$.

- Diffraction spots, once identified in the image stack via connected component labeling, are fit with two- or three-dimensional profile functions (as appropriate) in the angular space $\{2\theta, \eta, \omega\}$. Generally, elliptical gaussians are sufficient. This enhances both the accuracy of the spot centroids as well as the ability to measure integrated intensities of spots, the latter of which is important for determining the relative volume among a neighborhood of grains.

- A novel indexing scheme is utilized for scans in which full sample cross-sections are interrogated – and thus contain only fully complete grains – where only the orientations fibers underlying the spots from one or two $\{hkl\}$ are searched. As grains are indexed subject to tolerances on d-spacing ($\Delta d/d_0$), η, ω and completeness, their diffraction spots are removed from subsequent searches. If another grain attempts to claim a spot that has been previously claimed, the reflection is flagged as a potentially overlapped. Such overlapped spots are common in microstructures containing twins, and can be removed or otherwise post-processed once identified.

- Friedel pairs are used to refine the center-of-mass coordinates *independently* of the orientation and strain refinement.

- Orientation and strain refinement are accomplished through fitting a deformation gradient tensor, $\mathbf{F}$, that takes the reference (undeformed) primitive lattice vectors to the current (deformed) configuration. The subtle, yet critical, detail in solving for a

unique lattice orientation and strain tensor under the crystal symmetry is to employ the *left* polar decomposition: $\mathbf{F} = \mathbf{V} \cdot \mathbf{R}$. When applied in this order, $\mathbf{R}$, acts first on the reference lattice vectors, which are interpreted as being invariant under the crystal symmetry. In this sense, $\mathbf{R}$ is equivalent to the typical definition of the grain orientation and may be mapped to the associated fundamental zone of the orientation space. The six independent components of the symmetric positive-definite $\mathbf{V}$ then represent the stretch tensor components written in the sample frame. With $\mathbf{F}$ in hand, a strain measure can be readily calculated; examples include the (left) Green-Lagrange strain, $\frac{1}{2}(\mathbf{F}\mathbf{F}^T - \mathbf{I})$, the Biot strain, $\mathbf{V} - \mathbf{I}$, and the true strain, $\ln \mathbf{V}$.

3. FINITE ELEMENT MODELING

The data available from the far-field 3DXRD experiment lends itself particularly well to comparison with finite element-based polycrystal plasticity simulations. There have been many efforts trained on generating virtual microstructures, including vornoi tesselations and finite elements (Brahme, Alvi, Saylor, Fridy, and Rollett, 2006; St-Pierre, Héripré, Dexet, Crépin, Bertolino, and Bilger, 2008; Groeber, Ghosh, Uchic, and Dimiduk, 2008) A simple seeding algorithm was employed to generate the finite element mesh from the measured centroids. Starting with a regular three-dimensional grid of hexahedral elements, the grains – distinguished by their underlying lattice orientation – are "grown" isotropically. The growth rates are weighted by the measured relative volumes for each grain (*i.e.* relative to the centered reference grain), such that the simulated and measured relative volumes are as consistent as possible. The full mesh, and central portion containing the neighborhood of interest are depicted in Fig. 2.

A conventional crystal elasto-viscoplasticity material model is used in a finite element context to capture deformation response including intra-granular stress heterogeneity. The material model is based on a multiplicative decomposition of the deformation gradient and various aspects of the formulation are reported elsewhere (Barton and Dawson, 2001; Barton, Benson, and Becker, 2005; Barton, Winter, and Reaugh, 2009). Plastic deformation occurs by slip on a specific slip systems, with basal $\langle 2\bar{1}\bar{1}0\rangle\,\{0001\}$, $\langle \bar{2}110\rangle\,\{01\bar{1}0\}$, and $\langle \bar{2}113\rangle\,\{10\bar{1}1\}$ slip system families used herein. The pyramidal slip systems are comparatively resistant to slip, resulting in more deformation heterogeneity than in metals with cubic crystal symmetry. To capture this effect, we employ fixed ratios of slip system strengths. For simplicity, the basal and prismatic systems are assumed to have the same strength and the pyramidal systems have a strength 3.15 times higher, consistent with the range of experimental observations Lütjering and Williams (2003). Slip asymmetries and potential non-Schmid effects are neglected Jones and Hutchinson (1981).

An initially cube-shaped domain containing the experimentally measured grains in the central portion is created. The volume around the central neighborhood is filled with (incomplete) grains having orientations sampled from a uniform orientation distribution. The spatial discretization is such that each grain is composed of several thousand finite elements; this level of discretization facilitates a significant amount of intra-granular heterogeneity arising from both the grain-level anisotropy and neighborhood interactions. The elastic and plastic material parameters were adjusted to match the stress-strain data for the alloy, and the aggregate was subsequently deformed in uniaxial tension out to $\sim 2\%$ plastic strain as in the experiment. Standard solution methods are used, with eight point quadrature for element level volume integrals and an algebraic multi-grid method for parallel solution of the boundary value problem Henson and Yang (2002); Anderson et al. (2003).

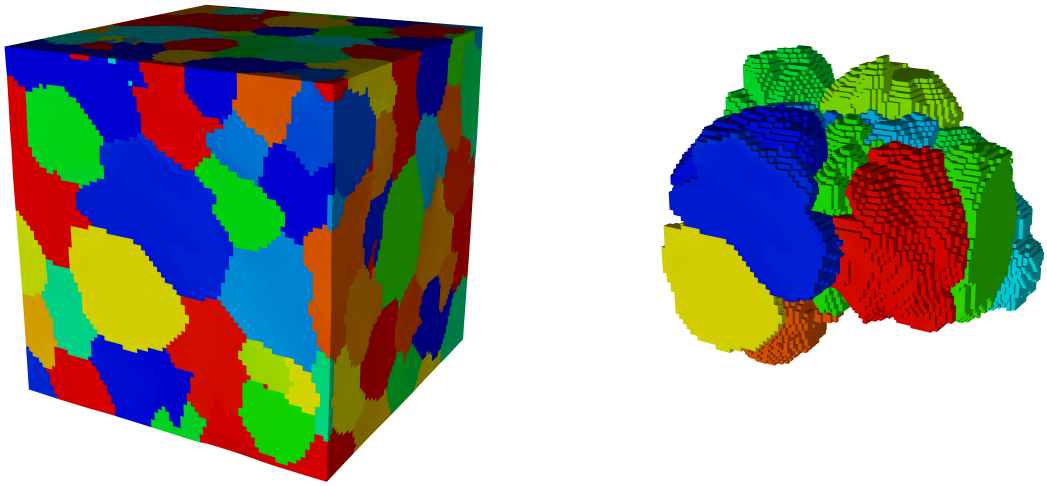

Fig. 2: Virtual polycrystalline aggregate (*left*) and the measured neighborhood (*right*)

4. RESULTS

Intra-granular stresses from two different grains in the simulation are illustrated in Fig. 3. For reference, the macroscopic strain was $\sim 2\%$, and the angle between the c-axis and tensile axis for each grain was 28.6° (*left*) and 75.2° (*right*). The top rows show the sections of (deviatoric) stress space spanned by the basal $\langle 2\bar{1}\bar{1}0\rangle\,\{0001\}$ and prismatic $\langle\bar{2}110\rangle\,\{01\bar{1}0\}$ slip systems; note that those slip systems each define two-dimensional surfaces in the full five-diensional space. The black lines represent the traces of the reference critical resolved shear stress (CRSS) values for each slip system, $\boldsymbol{\tau} : \mathbf{P}^\alpha = g^\alpha$, where $\boldsymbol{\tau}$ is the cauchy stress, $\mathbf{P}^\alpha$ is the deviator of the schmid tensor for the α^{th} slip system, and g^α are the corresponding initial CRSS values. These figures approximate yield surface sections at fixed state; edges correspond to facets, and vertices correspond to edges. The pyramidal slip systems do not describe a simple two-dimensional subspace, nor are they on average active in the incipient plasticity regime examined, and therefore are not shown. In each section, blue points are the projections of the stresses from each element discretizing the grain into the respective stress subspace. The red point is the projection of the stress obtained via the volume-averaged strain tensor for the grain, and thus approximates the type of stress available from the far-field 3DXRD experiment. Points near the envelop denote "active" slip systems under the power-law slip kinetics, and the spread is indicative of the intra-granular deformation heterogeneity. That the red points lie near the center of these clouds in not at all surprising; it does illustrate, however, that the average stress lies at a point that is consistent with the bulk slip system activity. For the grain with the c-axis at 28.6°, one basal slip system is active over the grain. For the grain at 75.2°, one basal and two prismatic slip systems are active. The bottom row in each panel in Fig. 3 shows two-dimensional histograms of slip activity over the grain for each denoted slip system. The color represents counts on a log scale plotted against normalized shearing rate, $\dot{\gamma}^\alpha / \|\mathbf{D}_a\|$ where $\mathbf{D}_a$ is the applied rate-of-deforamtion tensor, and resolved shear stress, $\tau^\alpha = \boldsymbol{\tau} : \mathbf{P}^\alpha$, for each slip system. The black lines along the τ^α axes represent the values calculated from the grain volume-averaged stress for each individual slip system. The shape of the histograms for active slip systems reflect the underlying power law kinetics and display a clear "knee" with high count densities around the CRSS values. The histograms for largely inactive slip systems generally lack

the knee and have peak counts along the tail at stress magnitudes below the corresponding CRSS value.

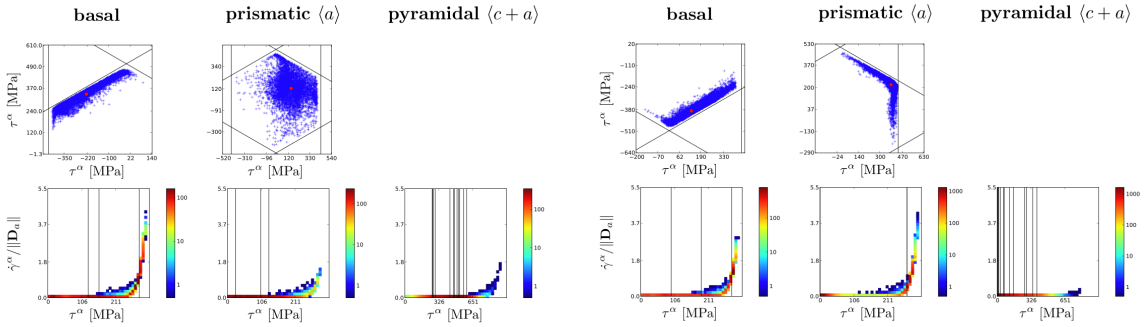

Fig. 3: Intra-granular stresses from two different grains in the simulation at $\sim 2\%$ macroscopic strain. The angle between the c-axis and the tensile axis for the grains are 28.6° (*left*) and 75.2° (*right*).

Inter-granular stress data over the grain neighborhood is shown in Fig. 4; composite histograms from the simulation are shown on the left, while histograms of measured τ^α are shown on the right. For the simulated data, the upper row corresponds to a ratio of basal:prismatic:pyramidal slip system strengths of 1:1:3.15, while the bottom row corresponds to the ratios 2:1:3.15. The colored two-dimensional histograms represent the aggregate of the grain-level histograms as shown in Fig. 3 over the neighborhood. The superimposed grey histograms represent the τ^α values calculated from the grain-averaged stresses over each slip system. Note that slip systems that are active over the neighborhood display $\dot{\gamma}^\alpha/\|\mathbf{D}_a\| - \tau^\alpha$ histograms consistent with the single-grain counterparts in Fig. 3: a clear knee with a high counting density at the CRSS value. What is interesting, however, is that the purely inter-granular histograms (*i.e.* the grey bars) *also* display a peak at a stress magnitude that coincides quite closely with the CRSS value. Meanwhile the histograms for the inactive pyramidal slip systems display no such peak at the tail. This is an important result: it indicates (within our modeling assumptions) that despite the intra-granular heterogeneity, the statistics over the volume-averaged stresses from each grain in the neighborhood are sufficient for capturing the underlying CRSS values. Furthermore, this character is preserved for histograms calculated from the simulation after a 20% (elastic) unloading*, the only salient difference being that the location of the peak moves down the stress axis by an amount equivalent to the magnitude of the unloading.

Using this result, the measured τ^α histograms from the experiment indicate that the basal slip systems are active in the sample with a CRSS value of ~ 260 MPa when the 15% unloading is considered. Neither the prismatic or pyramidal slip systems appear to be active on the whole. The pyramidal slip systems are expected to be $\sim 3\times$ stronger, and thus inactive at these macroscopic stress levels. The prismatic slip systems, however, are generally believed to be roughly the same strength as the basal slip systems at room temperature. For Ti-7%Al that has been air-cooled after annealing, it has been reported that the basal slip systems *may* be effectively strong than the prismatic due to the extensive short-range order of the Al; the experimental results appear to corroborate this. The simulated histograms for the 2:1:3.15 slip system strength ratio in Fig. 4 do as well, as the peak in basal histogram is clearly suppressed as compared to that from the 1:1:3.15 case. Further plastic deformation of

*often in the *in situ* test, a small unloading before a scan prevents creep and stress relaxation.

the aggregate would eventually activate the other slip systems, which should be observable in these histograms provided that the patterns could still be indexed.

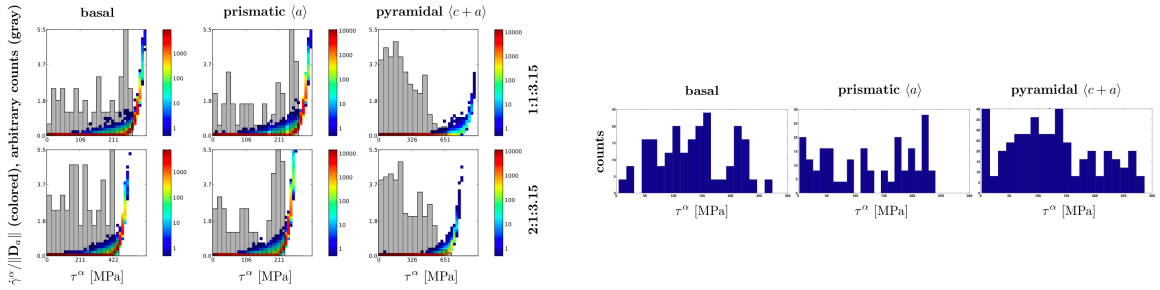

Fig. 4: Inter-granular stresses over the grain neighborhood. Virtual polycrystalline neighborhood (*left*) for two different ratios of slip system strengths, and experimental results (*right*) from air-cooled Ti-7%Al (Lienert et al., 2009). The experimental results agree more closely with the case having elevated basal slip system strength.

5. CONCLUSIONS

We have presented an application of the far-field 3DXRD technique to *in situ* measurements of micro-mechanical state in a deforming aggregate. With a fixed beam illuminating a contiguous neighborhood of grains, it is possible to determine the orientations, centroids, and mean strain states (*i.e.* lattice parameters) for each. From the ensemble of fully three-dimensional strain tensors, it is possible to statistically determine the critical resolved shear stresses for particular slip systems in a macroscopically yielded specimen *in situ*. In turn, with CRSS values in hand the slip activity for any individual grain may subsequently be determined. As the acquisition time is reduced by advances in detector technology, it will become possible to record many snapshots of the evolving inter-granular stress states under continuous loading through the elastic-plastic transition; in such detailed stress histories, it should be possible to detect when individual slip systems yield within a grain. When combined with the ensemble statistics, the technique becomes a powerful tool for studying plasticity in polycrystalline materials. Applications moving forward include the study of complex multi-phase alloys, geological materials, twinning, and phase transformations.

ACKNOWLEDGEMENT

This work performed under the auspices of the U.S. Department of Energy by Lawrence Livermore National Laboratory under Contract DE-AC52-07NA27344 (LLNL-JRNL-412144). Use of the Advanced Photon Source was supported by the U. S. Department of Energy, Office of Science, Office of Basic Energy Sciences, under Contract No. DE-AC02-06CH11357. MCB and MJM acknowledge the support of the National Science Foundation under CMMI-0800587. MPM gratefully acknowledges the Office of Naval Research, Julie Christodoulou, Grant Officer for support of this work as part of the D 3-D Program, contract number N00014-05-1-0505.

REFERENCES

Anderson, A., Cooper, R., Neely, R., Nichols, A., Sharp, R., Wallin, B., 2003. Users manual for ALE3D – an arbitrary Lagrange/Eulerian 3D code system. Tech. Rep. UCRL-MA-152204, Lawrence Livermore National Laboratory.

Aydıner, C. C., Bernier, J. V., Clausen, B., Lienert, U., Tomé, C. N., Brown, D. W., 2009. Evolution of stress in individual grains and twins in a magnesium alloy aggregate. Phys. Rev. B 80 (2), 024113(6).
URL http://dx.doi.org/10.1103/PhysRevB.80.024113

Barton, N. R., Benson, D. J., Becker, R., 2005. Crystal level continuum modelling of phase transformations: the $\alpha \leftrightarrow \epsilon$ transformation in iron 13, 707–731.
URL http://stacks.iop.org/0965-0393/13/707

Barton, N. R., Dawson, P. R., 2001. On the spatial arrangement of lattice orientations in hot-rolled multiphase titanium 9, 433–463.
URL http://stacks.iop.org/MSMSE/9/433

Barton, N. R., Winter, N. W., Reaugh, J. E., 2009. Defect evolution and pore collapse in crystalline energetic materials 17, 035003.
URL http://dx.doi.org/10.1088/0965-0393/17/3/035003

Bernier, J. V., Miller, M. P., Jun 2006. A direct method for the determination of the mean orientation-dependent elastic strains and stresses in polycrystalline materials from strain pole figures. Journal of Applied Crystallography 39 (3), 358–368.
URL http://dx.doi.org/10.1107/S0021889806009873

Bernier, J. V., Park, J. S., Pilchak, A. L., Glavicic, M. G., Miller, M. P., December 2008. Measuring stress distributions in ti-6al-4v using synchrotron x-ray diffraction. Metall. Mater. Trans. A 39 (13), 3120–3133.
URL http://dx.doi.org/10.1007/s11661-008-9639-6

Brahme, A., Alvi, M., Saylor, D., Fridy, J., Rollett, A., 2006. 3d reconstruction of microstructure in a commercial purity aluminum. Scripta Materialia 55 (1), 75 – 80, viewpoint set no. 41 "3D Characterization and Analysis of Materials" Organized by G. Spanos.
URL http://www.sciencedirect.com/science/article/B6TY2-4JT38T4-1/2/b1acfe40eee6e6be6399672c50ae905c

Groeber, M., Ghosh, S., Uchic, M. D., Dimiduk, D. M., 2008. A framework for automated analysis and simulation of 3d polycrystalline microstructures. part 2: Synthetic structure generation. Acta Materialia 56 (6), 1274 – 1287.
URL http://www.sciencedirect.com/science/article/B6TW8-4RS3TPM-1/2/5001f524a146ff26486f15a6dfbfdc39

Henson, V. E., Yang, U. M., 2002. Boomeramg: A parallel algebraic multigrid solver and preconditioner. Applied Numerical Mathematics 41, 155–177.

Jones, I. P., Hutchinson, W. B., 1981. Stress-state dependence of slip in titanium-6Al-4V and other h.c.p. metals 29, 951–968.

Lauridsen, E. M., Schmidt, S., Suter, R. M., Poulsen, H. F., December 2001. Tracking: a method for structural characterization of grains in powders or polycrystals. J. Appl. Cryst. 34, 744–750.
URL http://dx.doi.org/10.1107/S0021889801014170

Lienert, U., Brandes, M. C., Bernier, J. V., Weiss, J., Shastri, S. D., Mills, M. J., Miller, M. P., October 2009. In-situ single grain peak profile measurements on ti-7al during tensile deformation. Mat. Sci. Eng. A 524, 46–54.
URL http://dx.doi.org/10.1016/j.msea.2009.06.047

Lütjering, G., Williams, J. C., 2003. Titanium. Engineering Materials and Processes. Springer.

Margulies, L., Lorentzen, T., Poulsen, H. F., Leffers, T., April 2002. Strain tensor development in a single grain in the bulk of a polycrystal under load. Acta Mater. 50 (7), 1771–1779.
URL http://dx.doi.org/10.1016/S1359-6454(02)00028-9

Martins, R. V., Margulies, L., Schmidt, S., Poulsen, H. F., Leffers, T., 2004. Simultaneous measurement of the strain tensor of 10 individual grains embedded in an al tensile sample. Mat. Sci. Eng. A 387–389, 84–88.
URL http://dx.doi.org/10.1016/j.msea.2004.02.069

Poulsen, H. F., Nielsen, S. F., Lauridsen, E. M., Schmidt, S., Suter, R. M., Lienert, U., Margulies, L., Lorentzen, T., Juul Jensen, D., Dec 2001. Three-dimensional maps of grain boundaries and the stress state of individual grains in polycrystals and powders. Journal of Applied Crystallography 34 (6), 751–756.
URL http://dx.doi.org/10.1107/S0021889801014273

St-Pierre, L., Héripré, E., Dexet, M., Crépin, J., Bertolino, G., Bilger, N., 2008. 3d simulations of microstructure and comparison with experimental microstructure coming from o.i.m analysis. International Journal of Plasticity 24 (9), 1516 – 1532.
URL http://www.sciencedirect.com/science/article/B6TWX-4R53W82-1/2/f0d76a67ce56a97f78f254b472497017

Winther, G., 2008. Slip systems extracted from lattice rotations and dislocation structures. Acta Materialia 56 (9), 1919 – 1932.
URL http://www.sciencedirect.com/science/article/B6TW8-4S4S5TH-1/2/659068919518315dd6c72dfff59aed94